Supplementary Information

Supplementary Table 1. List of published compounds used in this study, related to **Fig. 2**.

Compound (alternative names)	Mammalian Target	Structure	Reference
AA26-3		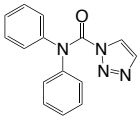	A. Adibekian *et al.*, Click-generated triazole ureas as ultrapotent in vivo-active serine hydrolase inhibitors. *Nat Chem Biol* **7**, 469-478 (2011).
AA26-7		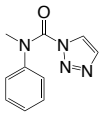	A. Adibekian *et al.*, Click-generated triazole ureas as ultrapotent in vivo-active serine hydrolase inhibitors. *Nat Chem Biol* **7**, 469-478 (2011).
AA26-8		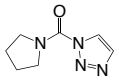	A. Adibekian *et al.*, Click-generated triazole ureas as ultrapotent in vivo-active serine hydrolase inhibitors. *Nat Chem Biol* **7**, 469-478 (2011).
AA26-9		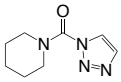	A. Adibekian *et al.*, Click-generated triazole ureas as ultrapotent in vivo-active serine hydrolase inhibitors. *Nat Chem Biol* **7**, 469-478 (2011).
AA39-2	PAFAH2	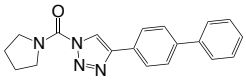	A. Adibekian *et al.*, Click-generated triazole ureas as ultrapotent in vivo-active serine hydrolase inhibitors. *Nat Chem Biol* **7**, 469-478 (2011).
AA39-3		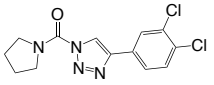	A. Adibekian *et al.*, Click-generated triazole ureas as ultrapotent in vivo-active serine hydrolase inhibitors. *Nat Chem Biol* **7**, 469-478 (2011).
AA44-2	ABHD11	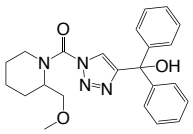	A. Adibekian *et al.*, Click-generated triazole ureas as ultrapotent in vivo-active serine hydrolase inhibitors. *Nat Chem Biol* **7**, 469-478 (2011).
AA74-1	APEH	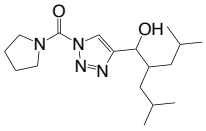	A. Adibekian *et al.*, Click-generated triazole ureas as ultrapotent in vivo-active serine hydrolase inhibitors. *Nat Chem Biol* **7**, 469-478 (2011).
ABC101		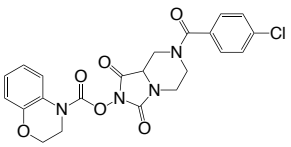	R. M. Suciu *et al.,* Selective Irreversible Inhibitors of the Wnt-Deacylating Enzyme NOTUM Developed by Activity-Based Protein Profiling. *ACS Med Chem Lett* **9**, 563-568 (2018).
ABC16		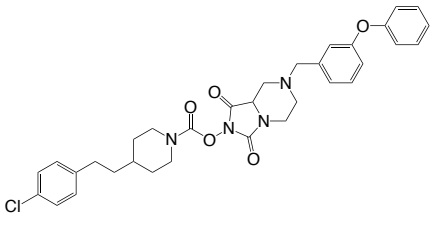	A. B. Cognetta, 3rd *et al.*, Selective N-Hydroxyhydantoin Carbamate Inhibitors of Mammalian Serine Hydrolases. *Chem Biol* **22**, 928-937 (2015).

ABC23	ABHD4	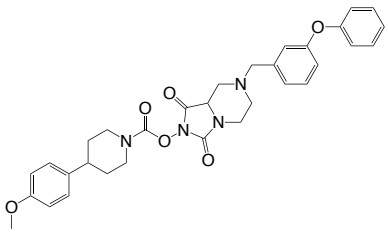	A. B. Cognetta, 3rd *et al.*, Selective N-Hydroxyhydantoin Carbamate Inhibitors of Mammalian Serine Hydrolases. *Chem Biol* **22**, 928-937 (2015).
ABC28	NOTUM	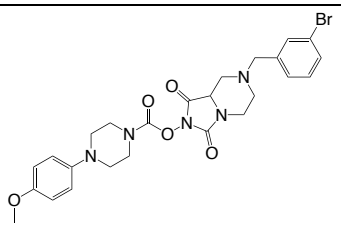	R. M. Suciu *et al.,* Selective Irreversible Inhibitors of the Wnt-Deacylating Enzyme NOTUM Developed by Activity-Based Protein Profiling. *ACS Med Chem Lett* **9**, 563-568 (2018).
ABC34	ABHD4, PPT1, PLA2G7	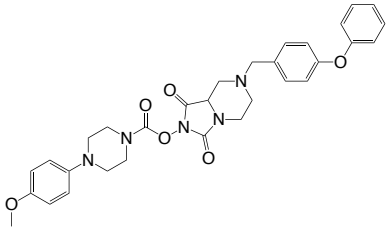	A. B. Cognetta, 3rd *et al.*, Selective N-Hydroxyhydantoin Carbamate Inhibitors of Mammalian Serine Hydrolases. *Chem Biol* **22**, 928-937 (2015).
ABC37		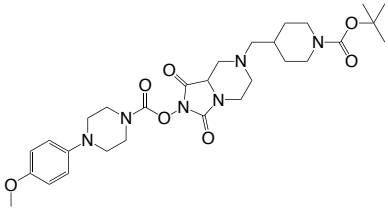	A. B. Cognetta, 3rd *et al.*, Selective N-Hydroxyhydantoin Carbamate Inhibitors of Mammalian Serine Hydrolases. *Chem Biol* **22**, 928-937 (2015).
ABC38		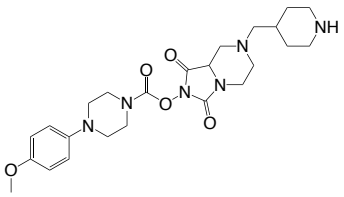	A. B. Cognetta, 3rd *et al.*, Selective N-Hydroxyhydantoin Carbamate Inhibitors of Mammalian Serine Hydrolases. *Chem Biol* **22**, 928-937 (2015).
ABC44	PPT1	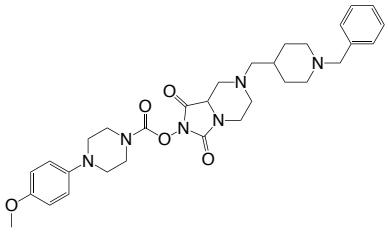	A. B. Cognetta, 3rd *et al.*, Selective N-Hydroxyhydantoin Carbamate Inhibitors of Mammalian Serine Hydrolases. *Chem Biol* **22**, 928-937 (2015).
ABC45	PPT1, DDHD2, LIPA, ABHD4	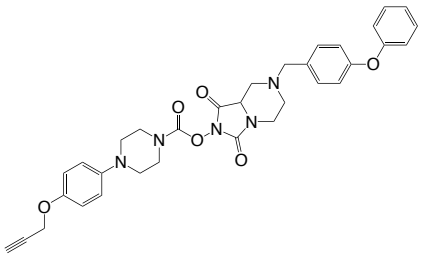	A. B. Cognetta, 3rd *et al.*, Selective N-Hydroxyhydantoin Carbamate Inhibitors of Mammalian Serine Hydrolases. *Chem Biol* **22**, 928-937 (2015).

ABC47	ABHD3/4	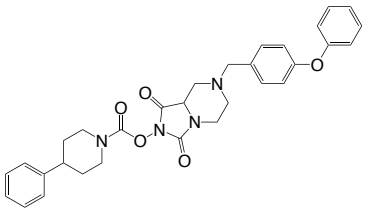	A. B. Cognetta, 3rd *et al.*, Selective N-Hydroxyhydantoin Carbamate Inhibitors of Mammalian Serine Hydrolases. *Chem Biol* **22**, 928-937 (2015).
ABC5		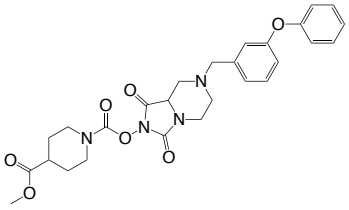	A. B. Cognetta, 3rd *et al.*, Selective N-Hydroxyhydantoin Carbamate Inhibitors of Mammalian Serine Hydrolases. *Chem Biol* **22**, 928-937 (2015).
ABC51		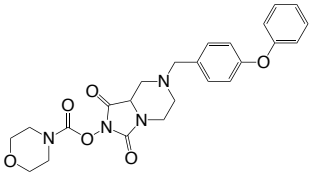	A. B. Cognetta, 3rd *et al.*, Selective N-Hydroxyhydantoin Carbamate Inhibitors of Mammalian Serine Hydrolases. *Chem Biol* **22**, 928-937 (2015).
ABC63	NOTUM	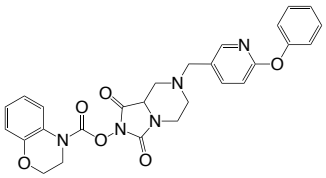	R. M. Suciu *et al.,* Selective Irreversible Inhibitors of the Wnt-Deacylating Enzyme NOTUM Developed by Activity-Based Protein Profiling. *ACS Med Chem Lett* **9**, 563-568 (2018).
ABC90	NOTUM, PPT1	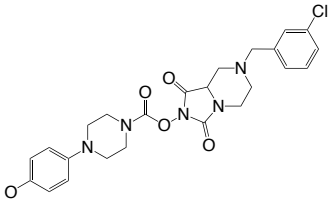	R. M. Suciu *et al.,* Selective Irreversible Inhibitors of the Wnt-Deacylating Enzyme NOTUM Developed by Activity-Based Protein Profiling. *ACS Med Chem Lett* **9**, 563-568 (2018).
ABC91		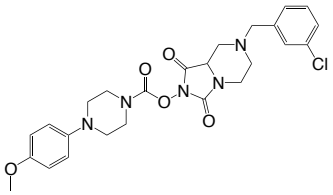	R. M. Suciu *et al.,* Selective Irreversible Inhibitors of the Wnt-Deacylating Enzyme NOTUM Developed by Activity-Based Protein Profiling. *ACS Med Chem Lett* **9**, 563-568 (2018).
ABC92	NOTUM	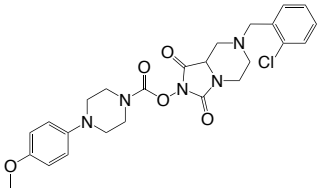	R. M. Suciu *et al.,* Selective Irreversible Inhibitors of the Wnt-Deacylating Enzyme NOTUM Developed by Activity-Based Protein Profiling. *ACS Med Chem Lett* **9**, 563-568 (2018).
ABC99	NOTUM	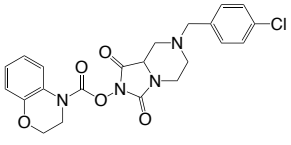	R. M. Suciu *et al.,* Selective Irreversible Inhibitors of the Wnt-Deacylating Enzyme NOTUM Developed by Activity-Based Protein Profiling. *ACS Med Chem Lett* **9**, 563-568 (2018).

ABL127	PPME1	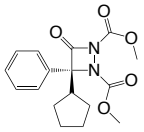	D. A. Bachovchin *et al.*, Academic cross-fertilization by public screening yields a remarkable class of protein phosphatase methylesterase-1 inhibitors. *Proc Natl Acad Sci U S A* **108**, 6811-6816 (2011).
ABL303	ABHD10	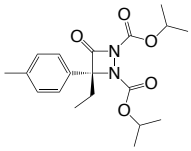	A. M. Zuhl et al., Competitive Activity-Based Protein Profiling Identifies Aza-β-Lactams as a Versatile Chemotype for Serine Hydrolase Inhibition. *J Am Chem Soc* **134**, 5068-5071 (2012).
AFK147 (57)	PNPLA4	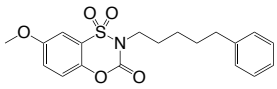	A. F. Kornahrens et al., Design of Benzoxathiazin-3-one 1,1-Dioxides as a New Class of Irreversible Serine Hydrolase Inhibitors: Discovery of a Uniquely Selective PNPLA4 Inhibitor. J Am Chem Soc 139, 7052-7061 (2017).
BIA 10-2474	FAAH	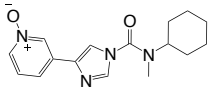	A. C. M. van Esbroeck *et al.*, Activity-based protein profiling reveals off-target proteins of the FAAH inhibitor BIA 10-2474. *Science* **356**, 1084-1087 (2017).
BIA 10-2639		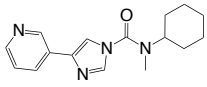	A. C. M. van Esbroeck *et al.*, Activity-based protein profiling reveals off-target proteins of the FAAH inhibitor BIA 10-2474. *Science* **356**, 1084-1087 (2017).
darapladib (SB-480848)		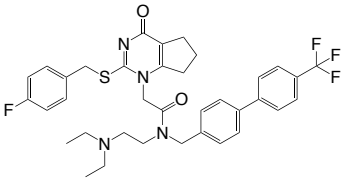	J. A. Blackie et al., The identification of clinical candidate SB-480848: a potent inhibitor of lipoprotein-associated phospholipase A2. *Bioorg Med Chem Lett* **13**, 1067-1070 (2003).
DH376	DAGLa	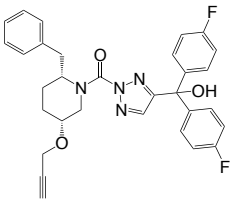	D. Ogasawara et al., Rapid and profound rewiring of brain lipid signaling networks by acute diacylglycerol lipase inhibition. *Proc Natl Acad Sci U S A* **113**, 26-33 (2016).
DO34	DAGLa, DAGLb	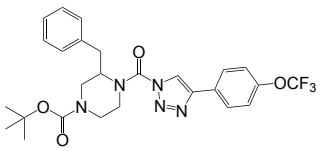	D. Ogasawara et al., Rapid and profound rewiring of brain lipid signaling networks by acute diacylglycerol lipase inhibition. *Proc Natl Acad Sci U S A* **113**, 26-33 (2016).
DO53		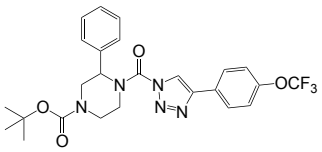	D. Ogasawara *et al.*, Rapid and profound rewiring of brain lipid signaling networks by acute diacylglycerol lipase inhibition. *Proc Natl Acad Sci U S A* **113**, 26-33 (2016).
JJH221		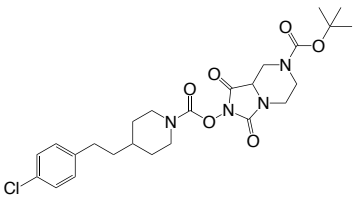	A. B. Cognetta, 3rd *et al.*, Selective N-Hydroxyhydantoin Carbamate Inhibitors of Mammalian Serine Hydrolases. *Chem Biol* **22**, 928-937 (2015).

JJH248		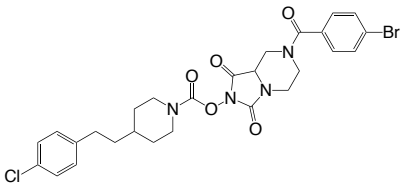	A. B. Cognetta, 3rd *et al.*, Selective N-Hydroxyhydantoin Carbamate Inhibitors of Mammalian Serine Hydrolases. *Chem Biol* **22**, 928-937 (2015).
JJH250		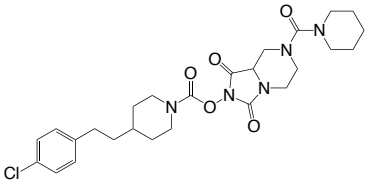	A. B. Cognetta, 3rd *et al.*, Selective N-Hydroxyhydantoin Carbamate Inhibitors of Mammalian Serine Hydrolases. *Chem Biol* **22**, 928-937 (2015).
JJH251	ABHD4, LYPLA1/2	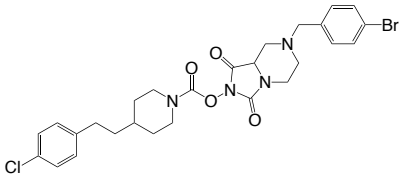	A. B. Cognetta, 3rd *et al.*, Selective N-Hydroxyhydantoin Carbamate Inhibitors of Mammalian Serine Hydrolases. *Chem Biol* **22**, 928-937 (2015).
JJH253		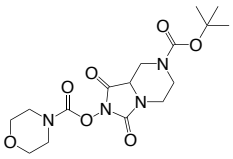	A. B. Cognetta, 3rd *et al.*, Selective N-Hydroxyhydantoin Carbamate Inhibitors of Mammalian Serine Hydrolases. *Chem Biol* **22**, 928-937 (2015).
JJH254	LYPLA1/2	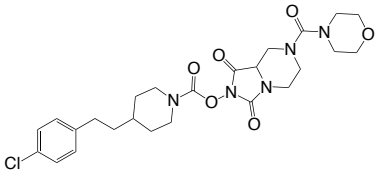	A. B. Cognetta, 3rd *et al.*, Selective N-Hydroxyhydantoin Carbamate Inhibitors of Mammalian Serine Hydrolases. *Chem Biol* **22**, 928-937 (2015).
JJH321		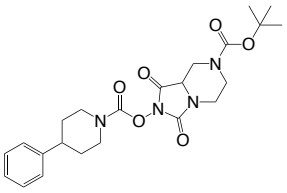	A. B. Cognetta, 3rd *et al.*, Selective N-Hydroxyhydantoin Carbamate Inhibitors of Mammalian Serine Hydrolases. *Chem Biol* **22**, 928-937 (2015).
JJH322		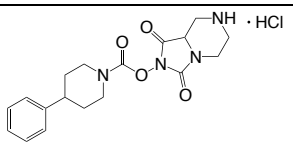	A. B. Cognetta, 3rd *et al.*, Selective N-Hydroxyhydantoin Carbamate Inhibitors of Mammalian Serine Hydrolases. *Chem Biol* **22**, 928-937 (2015).
JJH331		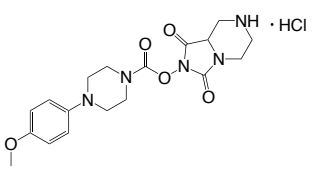	A. B. Cognetta, 3rd *et al.*, Selective N-Hydroxyhydantoin Carbamate Inhibitors of Mammalian Serine Hydrolases. *Chem Biol* **22**, 928-937 (2015).
JMN21 (ML256)	pPAFAH	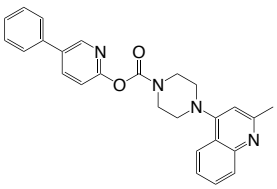	J. M. G. Nagano *et al.*, Optimization and characterization of a carbamate inhibitor for plasma platelet-activating factor acetylhydrolase (pPAFAH). *Probe Reports from the NIH Molecular Libraries Program*. (Bethesda (MD), 2011).

JT271-3 (4j)	ABHD3	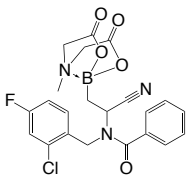	J. Tan et al., Multicomponent mapping of boron chemotypes furnishes selective enzyme inhibitors. Nat Commun 8, 1760 (2017).
JW1036		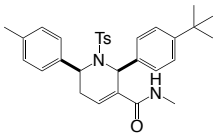	J. W. Chang *et al.*, Selective inhibitor of platelet-activating factor acetylhydrolases 1b2 and 1b3 that impairs cancer cell survival. *ACS Chem Biol* **10**, 925-932 (2015).
JW1038		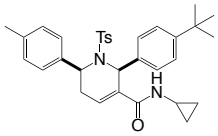	J. W. Chang *et al.*, Selective inhibitor of platelet-activating factor acetylhydrolases 1b2 and 1b3 that impairs cancer cell survival. *ACS Chem Biol* **10**, 925-932 (2015).
JW1039		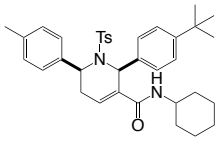	J. W. Chang *et al.*, Selective inhibitor of platelet-activating factor acetylhydrolases 1b2 and 1b3 that impairs cancer cell survival. *ACS Chem Biol* **10**, 925-932 (2015).
JW480	KIAA1363	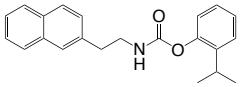	J. W. Chang, D. K. Nomura, B. F. Cravatt, A potent and selective inhibitor of KIAA1363/AADACL1 that impairs prostate cancer pathogenesis. *Chem Biol* **18**, 476-484 (2011).
JW651	MGLL	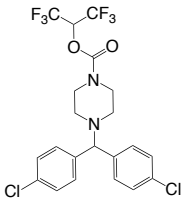	J. W. Chang, A. B. Cognetta, 3rd, M. J. Niphakis, B. F. Cravatt, Proteome-wide reactivity profiling identifies diverse carbamate chemotypes tuned for serine hydrolase inhibition. *ACS Chem Biol* **8**, 1590-1599 (2013).
JZL184	MGLL	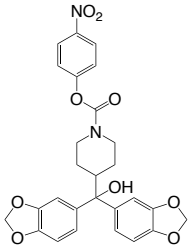	J. Z. Long *et al.*, Selective blockade of 2-arachidonoylglycerol hydrolysis produces cannabinoid behavioral effects. *Nat Chem Biol* **5**, 37-44 (2009).
KC01 (KC-6-30-1)	BAT5	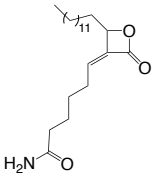	S. S. Kamat *et al.*, Immunomodulatory lysophosphatidylserines are regulated by ABHD16A and ABHD12 interplay. *Nat Chem Biol* **11**, 164-171 (2015).
KC02 (ML1-80-3)		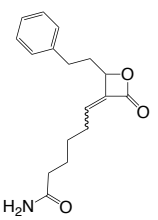	S. S. Kamat *et al.*, Immunomodulatory lysophosphatidylserines are regulated by ABHD16A and ABHD12 interplay. *Nat Chem Biol* **11**, 164-171 (2015).

KC03 (KC6-169-5)		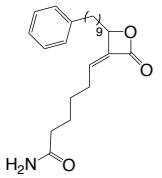	S. S. Kamat *et al.*, Immunomodulatory lysophosphatidylserines are regulated by ABHD16A and ABHD12 interplay. *Nat Chem Biol* **11**, 164-171 (2015).
KC05 (KC6-111-3)		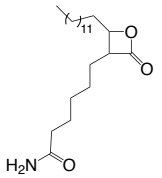	S. S. Kamat *et al.*, Immunomodulatory lysophosphatidylserines are regulated by ABHD16A and ABHD12 interplay. *Nat Chem Biol* **11**, 164-171 (2015).
KC07 (KC6-53-5)		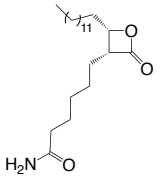	S. S. Kamat *et al.*, Immunomodulatory lysophosphatidylserines are regulated by ABHD16A and ABHD12 interplay. *Nat Chem Biol* **11**, 164-171 (2015).
KLH40		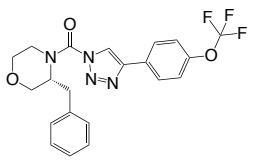	J. M. Inloes *et al.*, The hereditary spastic paraplegia-related enzyme DDHD2 is a principal brain triglyceride lipase. *Proc Natl Acad Sci U S A* **111**, 14924-14929 (2014).
KLH45b	DDHD2	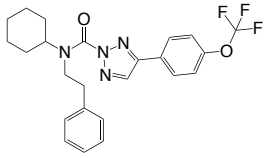	J. M. Inloes *et al.*, The hereditary spastic paraplegia-related enzyme DDHD2 is a principal brain triglyceride lipase. *Proc Natl Acad Sci U S A* **111**, 14924-14929 (2014).
KLH46 (36)		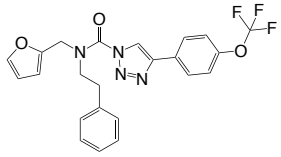	K. L. Hsu *et al.*, Development and optimization of piperidyl-1,2,3-triazole ureas as selective chemical probes of endocannabinoid biosynthesis. *J Med Chem* **56**, 8257-8269 (2013).
KML29	MGLL	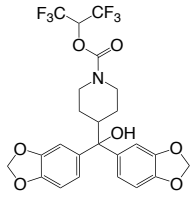	J. W. Chang *et al.*, Highly selective inhibitors of monoacylglycerol lipase bearing a reactive group that is bioisosteric with endocannabinoid substrates. *Chem Biol* **19**, 579-588 (2012).
KT109	DAGLb	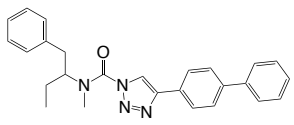	K. L. Hsu *et al.*, DAGLbeta inhibition perturbs a lipid network involved in macrophage inflammatory responses. *Nat Chem Biol* **8**, 999-1007 (2012).
KT116		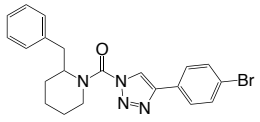	K. L. Hsu *et al.*, DAGLbeta inhibition perturbs a lipid network involved in macrophage inflammatory responses. *Nat Chem Biol* **8**, 999-1007 (2012).
KT117		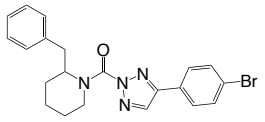	K. L. Hsu *et al.*, DAGLbeta inhibition perturbs a lipid network involved in macrophage inflammatory responses. *Nat Chem Biol* **8**, 999-1007 (2012).

KT172	DAGLa, DAGLb	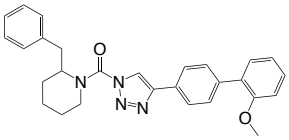	K. L. Hsu *et al.*, DAGLbeta inhibition perturbs a lipid network involved in macrophage inflammatory responses. *Nat Chem Biol* **8**, 999-1007 (2012).
KT185		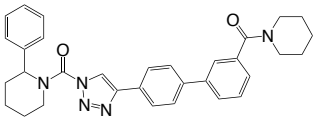	K. L. Hsu *et al.*, Discovery and optimization of piperidyl-1,2,3-triazole ureas as potent, selective, and in vivo-active inhibitors of alpha/beta-hydrolase domain containing 6 (ABHD6). *J Med Chem* **56**, 8270-8279 (2013).
KT186 (10)		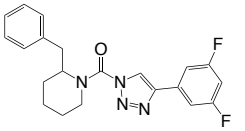	K. L. Hsu *et al.*, Development and optimization of piperidyl-1,2,3-triazole ureas as selective chemical probes of endocannabinoid biosynthesis. *J Med Chem* **56**, 8257-8269 (2013).
KT195	ABHD6	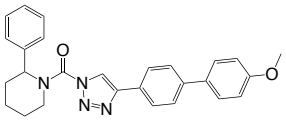	K. L. Hsu *et al.*, DAGLbeta inhibition perturbs a lipid network involved in macrophage inflammatory responses. *Nat Chem Biol* **8**, 999-1007 (2012).
KT203	ABHD6	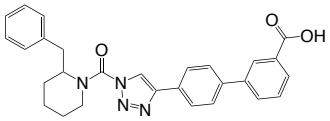	K. L. Hsu *et al.*, Discovery and optimization of piperidyl-1,2,3-triazole ureas as potent, selective, and in vivo-active inhibitors of alpha/beta-hydrolase domain containing 6 (ABHD6). *J Med Chem* **56**, 8270-8279 (2013).
MJN110	MGLL	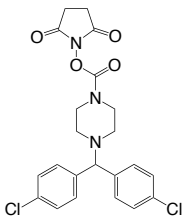	M. J. Niphakis *et al.*, Evaluation of NHS carbamates as a potent and selective class of endocannabinoid hydrolase inhibitors. *ACS Chem Neurosci* **4**, 1322-1332 (2013).
MJN193	ABHD6	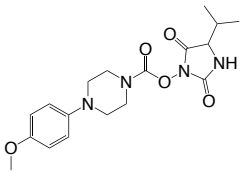	A. B. Cognetta, 3rd *et al.*, Selective N-Hydroxyhydantoin Carbamate Inhibitors of Mammalian Serine Hydrolases. *Chem Biol* **22**, 928-937 (2015).
MJN200	ABHD6	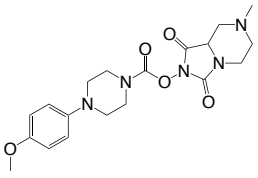	A. B. Cognetta, 3rd *et al.*, Selective N-Hydroxyhydantoin Carbamate Inhibitors of Mammalian Serine Hydrolases. *Chem Biol* **22**, 928-937 (2015).
MJN202		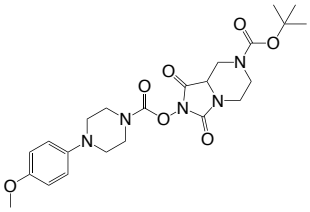	A. B. Cognetta, 3rd *et al.*, Selective N-Hydroxyhydantoin Carbamate Inhibitors of Mammalian Serine Hydrolases. *Chem Biol* **22**, 928-937 (2015).
P11	PAFAH1b2/3	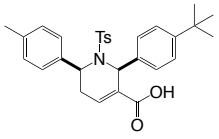	J. W. Chang *et al.*, Selective inhibitor of platelet-activating factor acetylhydrolases 1b2 and 1b3 that impairs cancer cell survival. *ACS Chem Biol* **10**, 925-932 (2015).

Palmostatin B (Palm B)	APT1/2	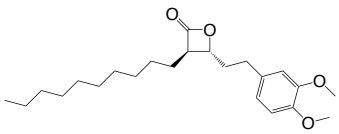	F. J. Dekker *et al.*, Small-molecule inhibition of APT1 affects Ras localization and signaling. *Nat Chem Biol* **6**, 449-456 (2010).
Palmostatin M (Palm M)	APT1/2	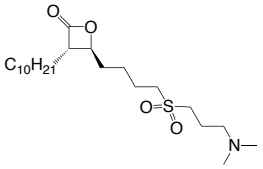	C. Hedberg *et al.*, Development of highly potent inhibitors of the Ras-targeting human acyl protein thioesterases based on substrate similarity design. *Angew Chem Int Ed Engl* **50**, 9832-9837 (2011).
PF-04457845	FAAH	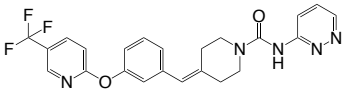	D. S. Johnson *et al.*, Discovery of PF-04457845: A Highly Potent, Orally Bioavailable, and Selective Urea FAAH Inhibitor. *ACS Med Chem Lett* **2**, 91-96 (2011).
THL	LIPF, PNLIP, CEL	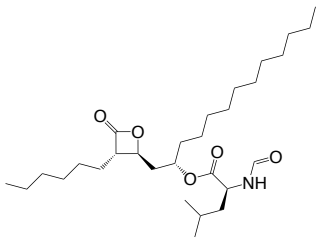	B. Borgstrom, Mode of action of tetrahydrolipstatin: a derivative of the naturally occurring lipase inhibitor lipstatin. *Biochim Biophys Acta* **962**, 308-316 (1988).
URB597	FAAH	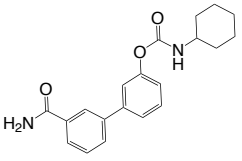	S. Kathuria, *et al*. Modulation of anxiety through blockade of anandamide hydrolysis. *Nat Med* **9**, 76-81 (2003).
WWL229	CES1D	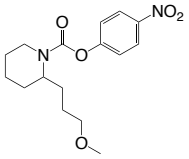	E. Dominguez *et al.*, Integrated phenotypic and activity-based profiling links Ces3 to obesity and diabetes. *Nat Chem Biol* **10**, 113-121 (2014).

Supplementary Table 2. 2-AG and AEA hydrolase activities of recombinant proteins following DMSO or JZL184 treatment (50 µM, 30 min pre-treatment) as quantified by LC-MS/MS, related to **Fig. 5** and **Supplementary Fig. 9**. Statistics were performed using two-sided Mann-Whitney test.

		Treatment				p-value (DMSO vs 50 µM JZL184)	p-value (METAP2 + DMSO vs protein + DMSO)
		DMSO		50 µM JZL184			
Protein	Species (substrate, product)	Mean (pmol /min /mg)	SE (pmol /min /mg)	Mean (pmol /min /mg)	SE (pmol /min /mg)		
METAP2 (n = 8)	2-AG (20:4), AA (20:4)	85.2	13.645	73.5	13.505	2.79E-01	
FAAH-1 (n = 6)	2-AG (20:4), AA (20:4)	108.8	24.215	101.6	23.056	8.18E-01	4.14E-01
FAAH-2 (n = 6)	2-AG (20:4), AA (20:4)	102.4	18.818	91.1	17.074	4.85E-01	4.14E-01
FAAH-3 (n = 4)	2-AG (20:4), AA (20:4)	214.1	41.463	152.7	51.213	3.43E-01	1.62E-02
FAAH-4 (n = 8)	2-AG (20:4), AA (20:4)	1200.8	209.728	121.2	24.812	1.55E-04	1.55E-04
FAAH-5 (n = 6)	2-AG (20:4), AA (20:4)	90.9	13.387	79.5	11.493	3.10E-01	4.14E-01
FAAH-6 (n = 6)	2-AG (20:4), AA (20:4)	103.0	20.003	88.8	19.812	4.85E-01	8.52E-01
Y41D4A.6 (n = 4)	2-AG (20:4), AA (20:4)	81.7	14.314	60.7	14.042	3.71E-01	>0.999999
Y53F4B.18 (n = 6)	2-AG (20:4), AA (20:4)	111.2	51.224	45.2	8.432	2.40E-01	5.73E-01
METAP2 (n = 8)	AEA (20:4), AA (20:4)	1.0	0.328	0.8	0.191	8.78E-01	
FAAH-1 (n = 6)	AEA (20:4), AA (20:4)	18.3	4.262	10.2	2.060	1.32E-01	6.66E-04
FAAH-2 (n = 6)	AEA (20:4), AA (20:4)	6.7	2.614	5.6	1.944	9.37E-01	7.99E-03
FAAH-3 (n = 4)	AEA (20:4), AA (20:4)	20.5	4.985	17.7	4.517	6.86E-01	4.04E-03
FAAH-4 (n = 8)	AEA (20:4), AA (20:4)	19.4	4.648	1.7	0.408	3.11E-04	1.55E-04
FAAH-5 (n = 6)	AEA (20:4), AA (20:4)	1.7	0.460	1.0	0.125	3.10E-01	2.82E-01
FAAH-6 (n = 6)	AEA (20:4), AA (20:4)	0.8	0.217	1.0	0.428	8.59E-01	9.50E-01
Y41D4A.6 (n = 4)	AEA (20:4), AA (20:4)	0.9	0.292	0.7	0.180	8.86E-01	>0.999999
Y53F4B.18 (n = 4)	AEA (20:4), AA (20:4)	23.0	6.070	1.3	0.379	2.86E-02	4.04E-03
METAP2 (n = 4)	2-AG (20:4), AA (20:4)	87.4	12.329	74.9	12.127	2.00E-01	
F13H6.13 (n = 4)	2-AG (20:4), AA (20:4)	166.8	23.495	84.5	16.989	5.71E-02	5.71E-02
F15A8.6 (n = 4)	2-AG (20:4), AA (20:4)	111.6	25.404	84.4	21.224	4.86E-01	4.86E-01
FAAH-4 (n = 4)	2-AG (20:4), AA (20:4)	1494.1	291.197	136.8	19.021	2.86E-02	2.86E-02
K11G9.2 (DMSO n = 3, JZL184 n = 4)	2-AG (20:4), AA (20:4)	94.1	36.373	82.4	19.307	8.57E-01	8.57E-01
Y71H2AM.13 (n = 4)	2-AG (20:4), AA (20:4)	118.7	32.524	91.4	19.765	6.86E-01	4.86E-01

Supplementary Table 3. Quantitative data of MAGs, NAEs and FFAs levels in L4 staged N2 and Δ*faah-4* animals as measured by targeted LC-MS/MS, related to **Fig. 6d** and **Supplementary Fig. 12a, b**. Statistics were performed using two-sided Mann-Whitney test.

	Strain				
	N2 (n = 6)		△*faah-4* (n = 7)		
Species	**Mean (pmol /mg protein)**	**SE (pmol /mg protein)**	**Mean (pmol /mg protein)**	**SE (pmol /mg protein)**	**p-value (N2 vs △*faah-4*)**
Monoacylglycerol (MAG)					
16:0	3.9	0.519	3.2	0.176	3.66E-01
18:0	2.0	0.190	2.1	0.120	4.45E-01
18:1	0.5	0.036	1.3	0.127	1.17E-03
18:2	0.4	0.028	1.1	0.110	1.17E-03
20:4	2.7	0.206	7.3	0.489	1.17E-03
20:5	6.4	0.557	16.2	1.099	1.17E-03
N-acylethanolamine (NAE)					
16:0	11.1	1.564	16.4	2.516	1.38E-01
16:1	4.1	0.647	4.3	0.589	7.31E-01
18:0	4.5	0.652	6.8	1.058	1.01E-01
18:1	0.2	0.006	0.2	0.011	3.50E-02
18:2	0.8	0.061	0.9	0.027	3.66E-01
20:4	0.1	0.009	0.1	0.010	7.34E-02
20:5	1.1	0.201	1.2	0.186	7.31E-01
Free fatty acid (FFA)					
16:0	69.7	6.240	60.9	2.629	4.45E-01
18:0	55.2	4.914	45.9	2.566	1.38E-01
18:1	15.7	2.104	14.4	1.556	>1.00E+00
18:2	8.2	0.836	8.6	1.538	7.31E-01
20:4	6.7	0.447	7.5	0.560	5.34E-01
22:6	0.8	0.058	0.9	0.027	6.28E-01

Supplementary Table 4. Quantitative data of MAGs, NAEs and FFAs levels in L4 staged N2 animals treated with DMSO or JZL184 (50 µM, 24 h) as measured by targeted LC-MS/MS, related to **Fig. 6e** and **Supplementary Fig. 12c, d**. Statistics were performed using two-sided Mann-Whitney test.

	Treatment				
	DMSO		50 µM JZL184		
Species	**Mean (pmol /mg protein)**	**SE (pmol /mg protein)**	**Mean (pmol /mg protein)**	**SE (pmol /mg protein)**	**p-value (DMSO vs 50 µM JZL184)**
Monoacylglycerol (MAG)	(n = 15)		(n = 10)		
16:0	2.2	0.181	2.6	0.183	1.78E-01
18:0	2.4	0.159	2.7	0.463	8.49E-01
18:1	1.0	0.126	2.2	0.244	3.02E-04
18:2	1.1	0.092	1.9	0.135	5.93E-05
20:4	6.8	0.453	11.1	0.796	1.19E-04
20:5	15.0	1.308	20.9	1.308	4.44E-03
N-acylethanolamine (NAE)	(n = 15)		(n = 10)		
16:0	13.0	2.134	13.6	2.332	8.49E-01
16:1	5.1	0.450	6.2	0.764	3.97E-01
18:0	6.5	0.629	6.5	0.863	9.78E-01
18:1	0.2	0.018	0.2	0.013	4.28E-01
18:2	0.7	0.074	1.1	0.091	5.40E-03
20:4	0.1	0.011	0.1	0.006	1.29E-01
20:5	0.9	0.171	1.0	0.102	1.60E-01
Free fatty acid (FFA)	(n = 14)		(n = 9)		
16:0	31.6	4.648	29.6	3.465	9.75E-01
18:0	36.2	6.093	33.4	3.733	8.77E-01
18:1	14.5	2.536	12.3	1.730	8.77E-01
18:2	8.5	1.491	8.1	1.224	>1.00E+00
20:4	10.8	1.177	8.4	1.083	0.201003
22:6	1.0	0.091	1.2	0.103	2.77E-01

Supplementary Table 5. Quantitative data of MAGs, NAEs and FFAs levels in L4 staged N2 and ∆*y53f4b.18* animals as measured by targeted LC-MS/MS, related to **Supplementary Fig. 12e-g**. Statistics were performed using two-sided Mann-Whitney test.

	Strain				
	N2		△*y53f4b.18*		
Species	**Mean (pmol /mg protein)**	**SE (pmol /mg protein)**	**Mean (pmol /mg protein)**	**SE (pmol /mg protein)**	**p-value (N2 vs △*y53f4b.18*)**
Monoacylglycerol (MAG)	(n = 8)		(n = 8)		
16:0	17.8	3.165	26.6	3.778	1.30E-01
18:0	42.5	6.797	64.1	8.428	1.05E-01
18:1	1.4	0.196	1.9	0.367	2.79E-01
18:2	0.8	0.072	1.2	0.088	1.48E-02
20:4	3.3	0.581	5.2	0.794	1.05E-01
20:5	11.5	2.137	17.9	3.096	1.30E-01
N-acylethanolamine (NAE)	(n = 8)		(n = 8)		
16:0	27.8	4.579	28.3	6.001	>0.999999
16:1	5.4	0.467	8.0	0.660	6.99E-03
18:0	22.4	4.535	21.9	4.859	7.98E-01
18:1	0.1	0.015	0.2	0.034	1.30E-01
18:2	0.4	0.022	0.7	0.123	3.82E-01
20:4	0.1	0.008	0.2	0.040	1.95E-01
20:5	1.7	0.223	2.4	0.282	1.05E-01
Free fatty acid (FFA)	(n = 9)		(n = 8)		
16:0	14.5	2.241	17.5	3.221	6.06E-01
18:0	11.2	1.564	12.8	1.427	4.23E-01
18:1	6.2	1.649	7.1	1.789	8.15E-01
18:2	2.2	0.316	2.5	0.250	4.81E-01
20:4	4.6	0.763	5.9	0.382	1.67E-01
22:6	0.2	0.020	0.2	0.032	4.81E-01

Supplementary Table 6. List of primers used in this study, related to **Fig. 3** and **4** and **Supplementary Fig. 7**, **9-11**, and **12**.

Gene	Sequence (5´ to 3´)	Primer	Experiment
faah-4	ACGCGTCGACGCCACCATGGGGAATAACTTCTGGTCTACGTGGTC	Fwd	cloning into pRK5
	AAGGAAAAAAGCGGCCGCATGAAGAAGATTAACACGTTCGAAATG	Rev	
f13h6.3	ACGCGTCGACGCCACCATGGGTGGATTCTTGTCTCATCTGA	Fwd	cloning into pRK5
	AAGGAAAAAAGCGGCCGCAATCTTTGCCGACTTCTTCTTTCCATAG	Rev	
f15a8.6	ACGCGTCGACGCCACCATGGGTGGTGTCATTTCATTCATAT	Fwd	cloning into pRK5
	AAGGAAAAAAGCGGCCGCGACGTTCTTTGAAGTAATCTTAATTTTC	Rev	
y71h2am.13	ACGCGTCGACGCCACCATGGGAGGAACAGTTTCAAAGCATA	Fwd	cloning into pRK5
	AAGGAAAAAAGCGGCCGCGAGATTCGGCGGTGGTCTGG	Rev	
faah-1	ACGCGTCGACGCCACCATGATTTTTTACTTGGTGCTTC	Fwd	cloning into pRK5
	AAGGAAAAAAGCGGCCGCTTTCCCAGTGACTGCGATTTC	Rev	
faah-2	AAGGAAAAAAGCGGCCGCATGTTATTACTACTATTCACTG	Fwd	cloning into pRK5
	ACGCGTCGACGCCACCATGTTATTACTACTATTCACTG	Fwd	
	AAGGAAAAAAGCGGCCGCTTTTCCGGTGACACCGCGTTC	Rev	
	ATGGACCAATGTCCACGAGAGTGGAA	Fwd	mutagenesis of SalI
	CATTTGAATTAATCAAAGGTCTTCCC	Rev	
faah-3	ACGCGTCGACGCCACCATGTGGTTTTTCTACGTCGC	Fwd	cloning into pRK5
	AAGGAAAAAAGCGGCCGCATGTGTTCTACTATACAATCCG	Rev	
faah-5	ACGCGTCGACGCCACCATGTCCAAAATGGAGGATAAG	Fwd	cloning into pRK5
	AAGGAAAAAAGCGGCCGCTTTCTTTGGAGCAATCTTCTTC	Rev	
faah-6	AAGGAAAAAAGCGGCCGCATGGGGAATATTCATCAAAAAACC	Fwd	cloning into pRK5
	ACGCGTCGACGCCACCATGGGGAATATTCATCAAAAAACC	Fwd	
	AAGGAAAAAAGCGGCCGCAAATCCTTTCGGGTTACTCATTG	Rev	
	CCAACGGCCAGTGGACTCGAATTTTA	Fwd	mutagenesis of SalI
	GTCTTGAAAAACATCTGTGCAACTTG	Rev	
y53f4b.18	ACGCGTCGACGCCACCATGGCGGTGCCGTATCGCC	Fwd	cloning into pRK5
	AAGGAAAAAAGCGGCCGCAAGTGGTCCAGCAGGAGTCCATC	Rev	
y41d4a.6	ACGCGTCGACGCCACCATGCACAGAATCGAAAGTTC	Fwd	cloning into pRK5
	AAGGAAAAAAGCGGCCGCTTTCCGAATTAAACCATCC	Rev	
	GATTTAGGTGACACTATAG	Fwd	sequencing pRK5
	TGTAACCATTATAAGCTG	Rev	
	CGTGTCGAGACCCAGTAACG	Fwd	genotyping for *faah-4* deletion
	GCGCCTTAATGGCATGAATA	Rev	
	CGAAGGAGATTTGCTTCTGAAA	Fwd	
	ACCGACGGTATCCTGCTCTT	Fwd	genotyping for *y53f4b.18* deletion
	GAGACCTTTGGATATTTGTTGGA	Rev	
	TAACCGTTGCCTTGCTCTCT	Fwd	

Supplementary Figures

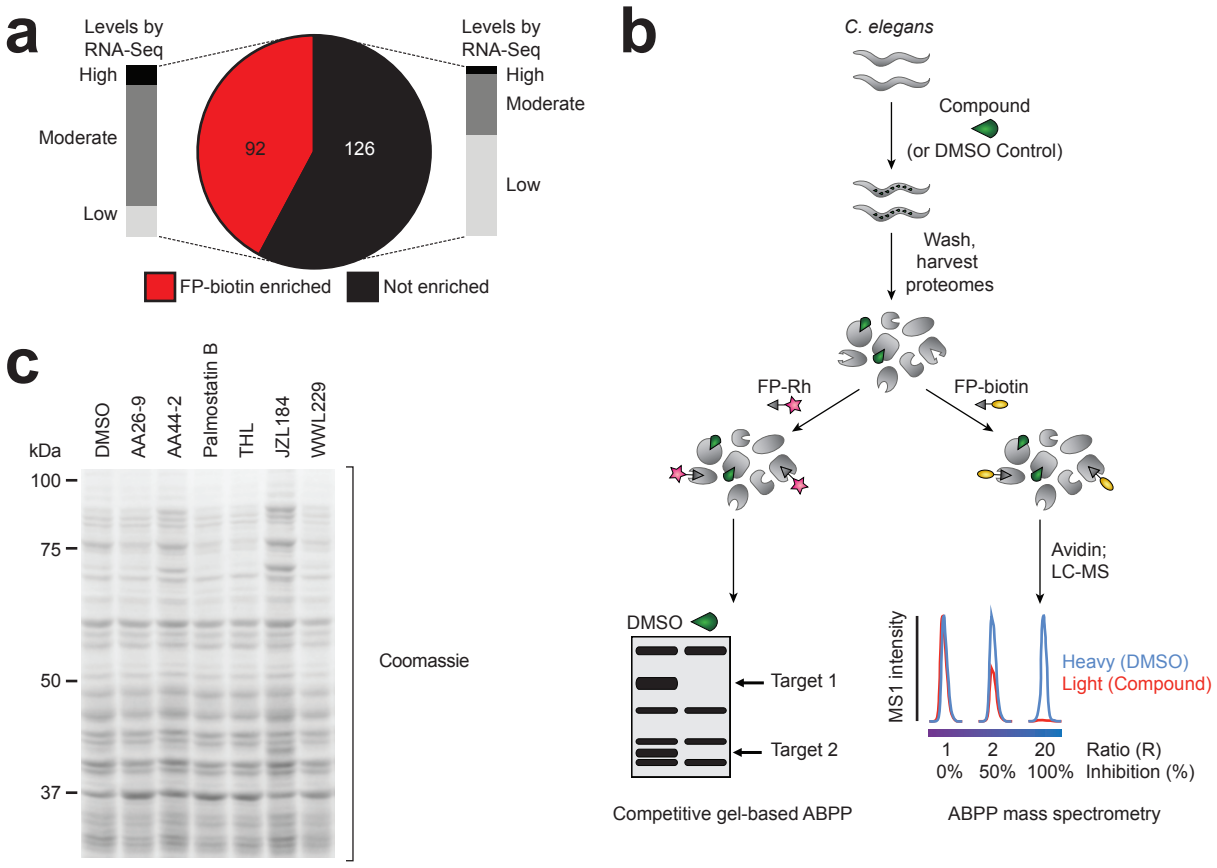

Supplementary Figure 1. (**a**) 92 (42%) of the 218 predicted SHs in *C. elegans* were enriched and identified by the FP-biotin probe. Also summarized are relative expression levels of FP-biotin-enriched or not enriched SHs as estimated by RNA-Seq[1]. (**b**) General schematic for the identifying targets of SH-directed inhibitors in *C. elegans* by competitive ABPP. Animals are treated with DMSO (control) or compound for 24 h *in vivo*, extensively washed to remove compound, and homogenized. Lysates are then either incubated with 1) FP-rhodamine and SH activities visualized by SDS-PAGE and in-gel fluorescence scanning, where loss of a fluorescent signal indicates SH inhibition by the test compound; or 2) FP-biotin for enrichment and identification of inhibitor-sensitive SHs by MS-based ABPP experiments, where animals are first isotopically labelled with heavy ^{15}N or light ^{14}N Op50 bacteria, and then treated with DMSO or compound for 24 h, respectively. After homogenization, heavy and light proteomes are combined, incubated with FP-biotin, and FP-reactive proteins enriched by avidin chromatography and identified and quantified by MS. Peptides with high heavy-to-light ratios designate SHs that are inhibited by the test compound. (**c**) Coomassie stain of fluorescent ABPP gel associated with **Fig. 1d** is representative of 2 independent experiments.

1 Rangaraju, S. *et al.* Suppression of transcriptional drift extends C. elegans lifespan by postponing the onset of mortality. *Elife* **4**, e08833, doi:10.7554/eLife.08833 (2015).

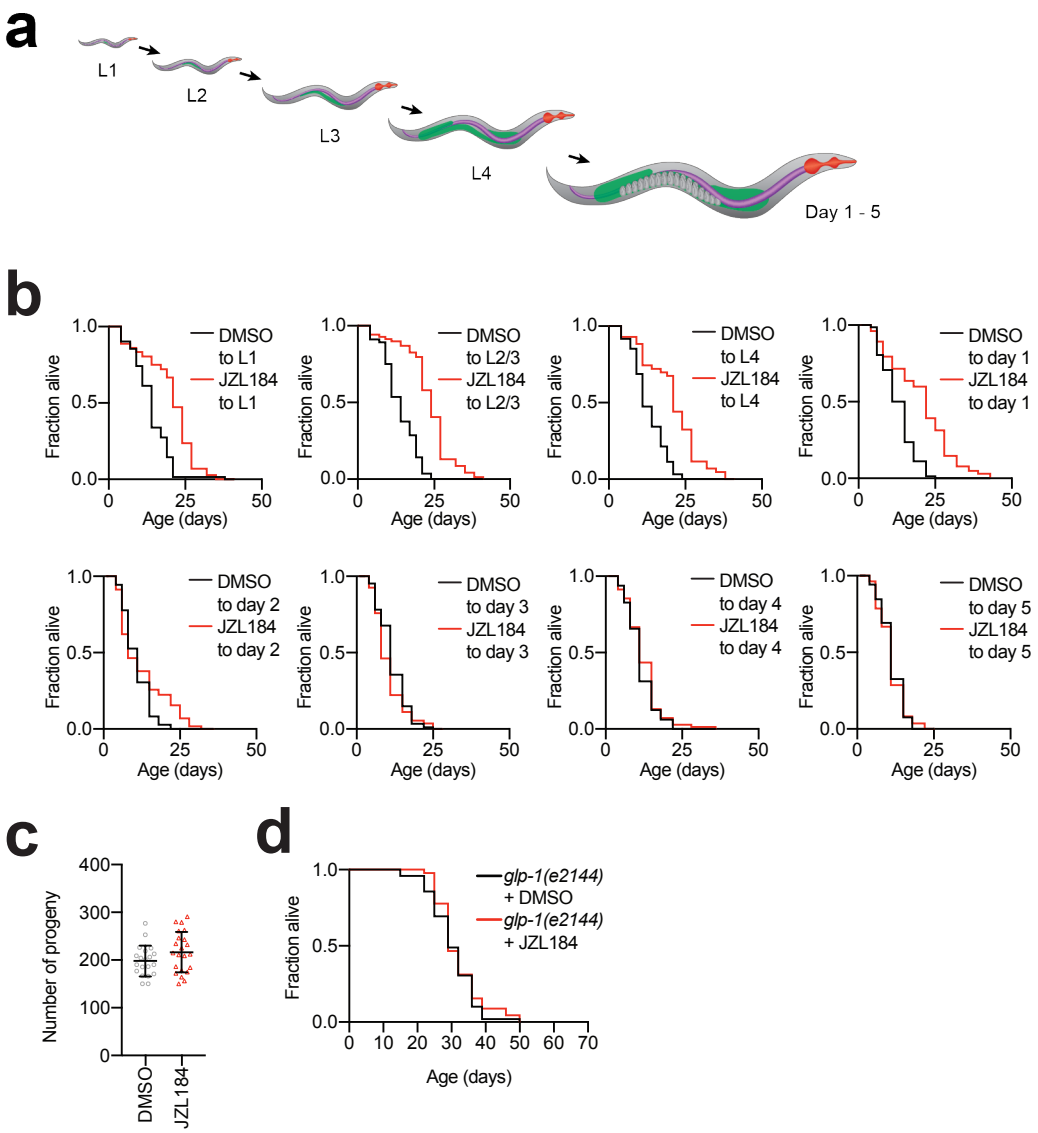

Supplementary Figure 2. JZL184 treatment during *C. elegans* development and early adulthood extends lifespan. (**a**) Illustration of *C. elegans* developmental stages. (**b**) Worms at distinct developmental stages were administered a single dose of JZL184 (50 μM). Stages included larval (L1, L2/3, and L4), reproductive (day 1 to 4 adult), and post-reproductive stages (day 5 adult). *C. elegans* treated with JZL184 past the first half of the reproductive stage did not experience a significant increase in lifespan. The data are representative of 3 (L1, L2/3, L4, day 2-4), 5 (day 5) or 6 (day 1) independent experiments (at least 28 worms per condition). Two-sided Mantel-Haenszel version of the log-rank test performed relative to DMSO control. (**c**) Brood size analysis of N2 worms treated with DMSO control or JZL184 (50 μM). *C. elegans* were maintained in liquid culture and transferred daily until day 5 to measure the number of progeny. Data is represented as mean ± s.d. (DMSO $n = 20$, JZL184 $n = 22$, $P = 0.1258$, two-sided unpaired t test). Data are from 4 independent experiments. (**d**) Lifespan curve of *glp-1(e1244)* mutant worms treated with FUDR and DMSO or JZL184 (50 μM) *glp-1* (DMSO $n = 49$ worms, JZL184 $n = 45$ worms, $P = 0.4170$ compared to *glp-1* DMSO control, two-sided Mantel-Haenszel version of the log-rank test). For **d**, results are representative of 2 independent experiments. Statistics for **b** and **d** are provided in **Supplementary Dataset 2.**

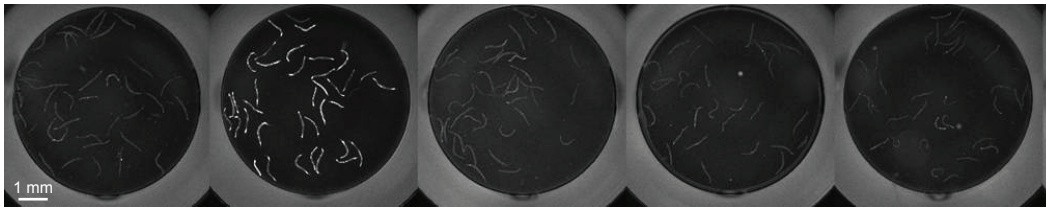

Supplementary Figure 3. JZL184 does not induce endoplasmic reticulum UPR.
Representative fluorescence microscopy images of *hsp-4::gfp* animals treated with the indicated concentrations of JZL184 for 24 h. Tunicamycin (5 μg/mL) was used as a positive control for visualizing induction of the endoplasmic reticulum UPR. Data is representative of 2 independent experiments.

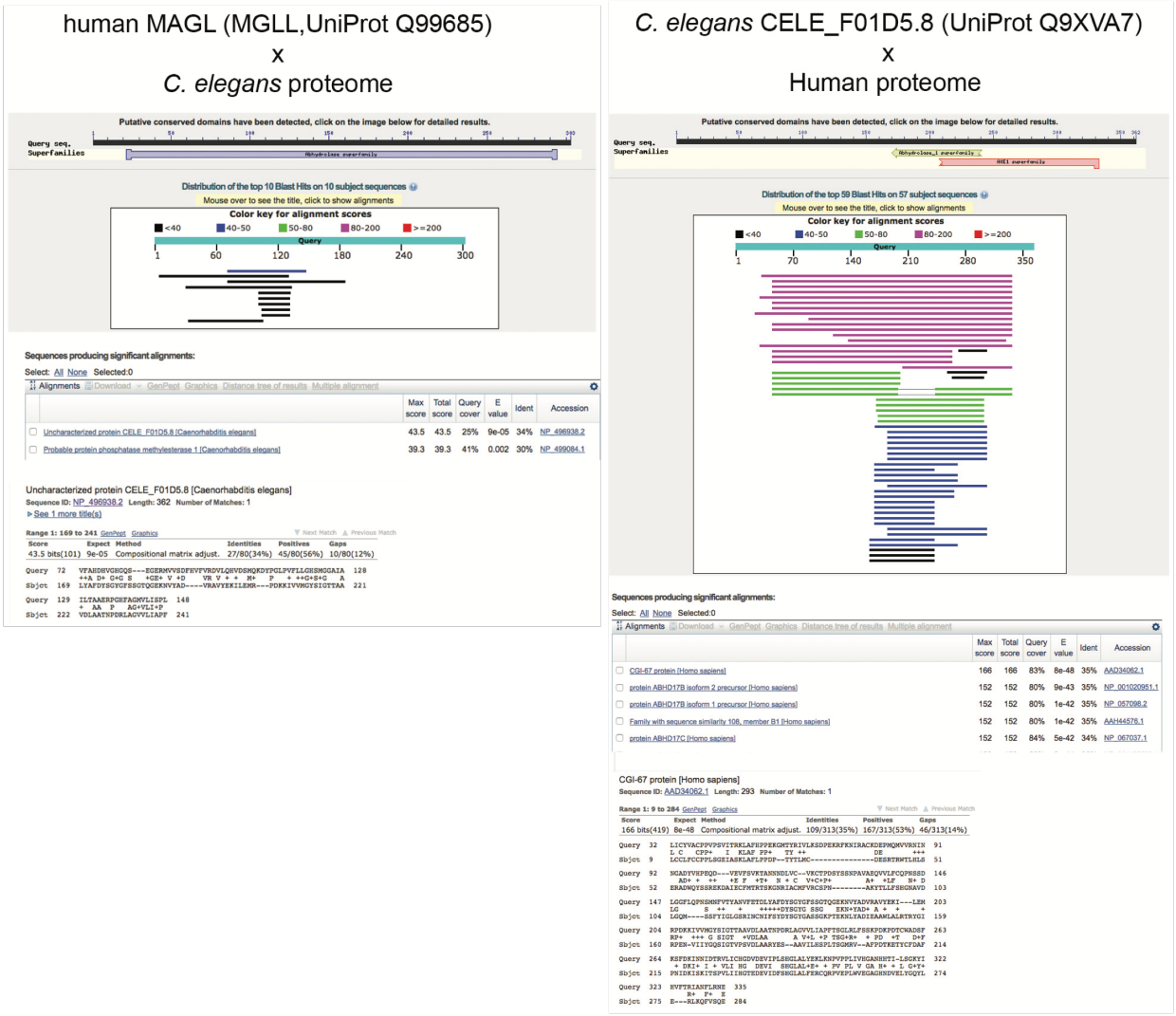

Supplementary Figure 4. BLAST search reveals that *C. elegans* lacks an orthologue of human MAGL (or MGLL). BLAST searching the protein sequence for human MAGL against the *C. elegans* database returned a weak homology match (34% identity across only 25% of the MAGL protein sequence) to F01D5.8 (left panels). A reciprocal BLAST search of the protein sequence for F01D5.8 against the human database revealed that this protein is an orthologue of the CGI-67/ABHD17 sub-clan of SHs (right panels), for which a much higher homology was observed (35% identity across ~90% of the CGI-67 protein sequence).

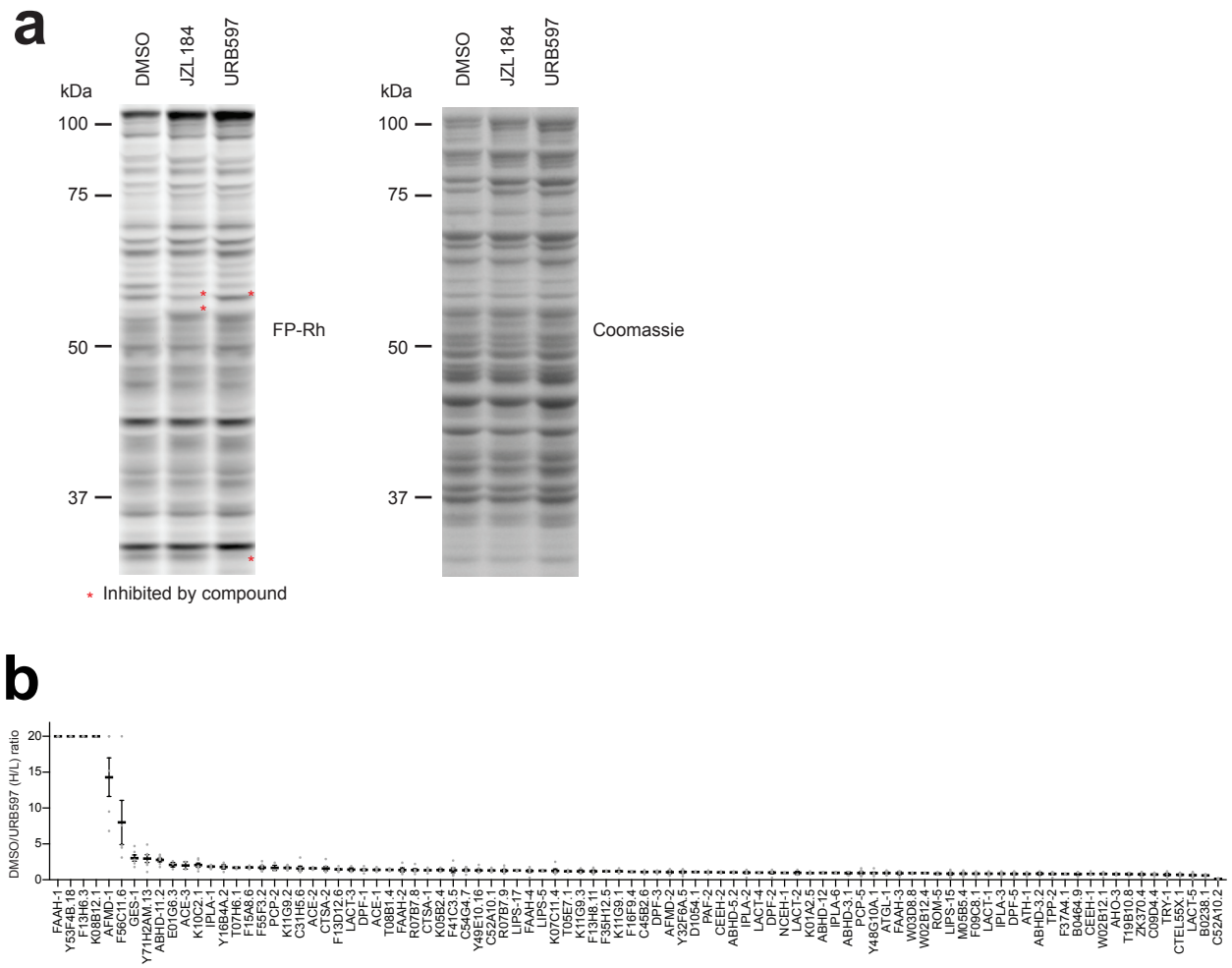

Supplementary Figure 5. URB597 inhibitory profile in *C. elegans in vivo*. (**a**) Gel-based ABPP of *C. elegans* proteins inhibited by JZL184 or URB597 (50 μM, 24 h) *in vivo* as measured by FP-rhodamine. Data is representative of 2 independent experiments. (**b**) FP-biotin enrichment and identification of SHs endogenously inhibited by URB597 (50 μM, 24 h) in *C. elegans*. MS-ABPP experiments were performed as described in the legend to **Fig. 3** and in the **Online Methods**. Data represent the mean of median ratios + s.e.m. for peptides quantified for each protein (*n* = 3 independent experiments).

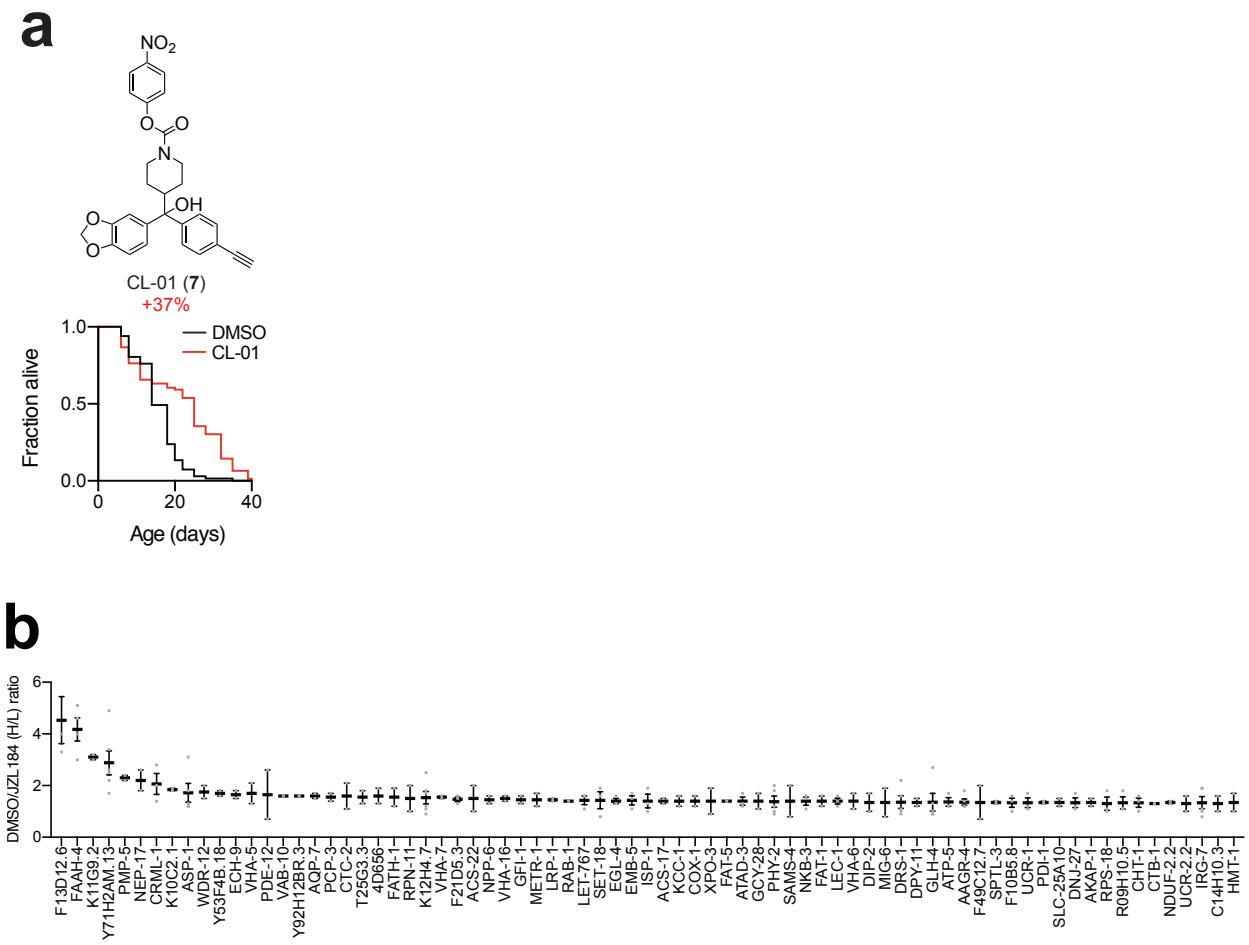

Supplementary Figure 6. Proteomic analysis with CL-01 (7) probe. (**a**) The CL-01 probe, a clickable analogue of JZL184, substantially extends lifespan. Kaplan-Meier plot revealing ~40% lifespan extension by CL-01 (50 μM) (DMSO *n* = 67, CL-01 *n* = 76, *P* = 1.20E-06 compared DMSO control, two-sided Mantel-Haenszel version of the log-rank test). The result is representative of 4 independent experiments. Statistics for **a** are provided in **Supplementary Dataset 2.** (**b**) Competitive MS-ABPP analysis showing the *in vivo* inhibition profile for JZL184 measured with the CL-01 probe. Isotopically labeled ^{15}N or light ^{14}N animals were treated with JZL184 (50 μM) or DMSO, respectively, on day 1 of adulthood for 24 h and CL-01 (50 μM, 18 h), followed by copper-catalyzed azide-alkyne cycloaddition (CuAAC or click) chemistry[2] conjugation to biotin-azide. Ratios shown for top 75 proteins. Data represent the mean of median ratios + s.e.m. for peptides quantified for each protein (*n* = 3 independent experiments).

2 Rostovtsev, V. V., Green, L. G., Fokin, V. V. & Sharpless, K. B. A stepwise huisgen cycloaddition process: copper(I)-catalyzed regioselective "ligation" of azides and terminal alkynes. *Angew Chem Int Ed Engl* **41**, 2596-2599, doi:10.1002/1521-3773(20020715)41:14<2596::AID-ANIE2596>3.0.CO;2-4 (2002).

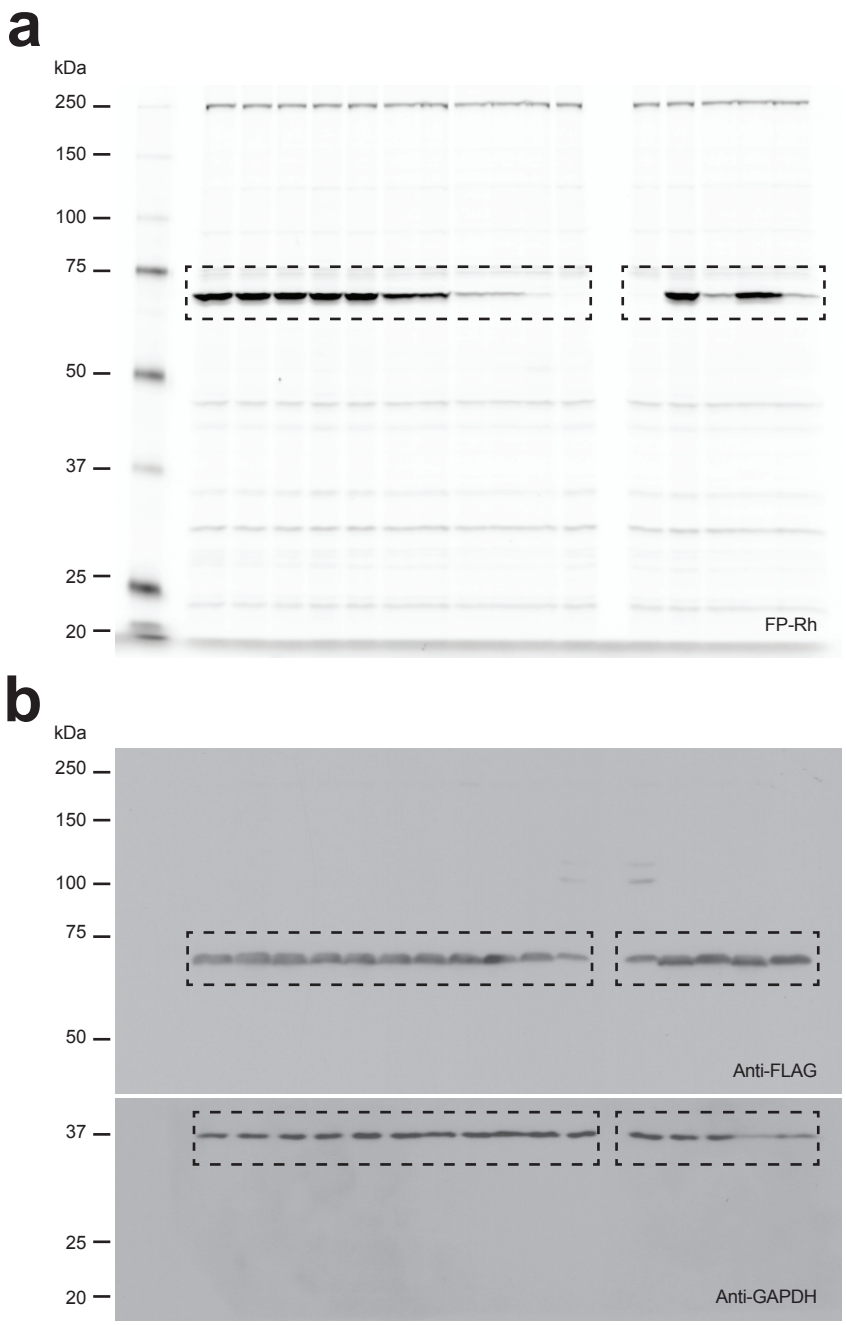

Supplementary Figure 7. Full length images of (**a**) FP-Rh or (**b**) Western blot analysis of FLAG-FAAH-4 or GAPDH in lysate samples. Data are representative of 3 independent samples. Cropped gel data for right and left lanes are shown in **Fig. 4c** and **4d**, respectively.

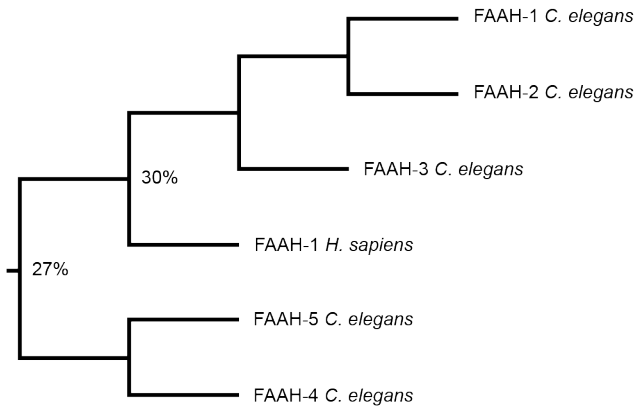

Supplementary Figure 8. Homology between amidases. Dendrogram depicting relatedness of *C. elegans* FAAHs to human FAAH-1. Note that human FAAH-1 is near-equally related (27-30%) to the various *C. elegans* FAAH proteins.

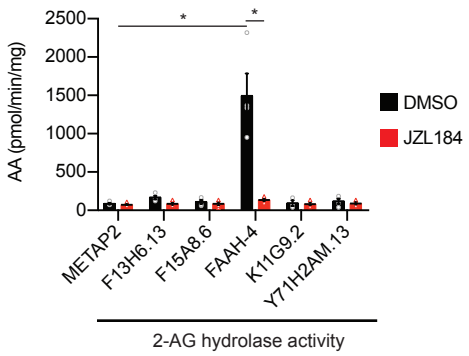

Supplementary Figure 9. 2-AG hydrolytic activity of SHs inhibited by JZL184 in vivo. Recombinant SHs or control protein METAP2 (5 µg of lysate) were expressed by transient transfection in HEK293T cells and their 2-AG hydrolytic activities measured in presence of JZL184 (50 µM, 30 min pre-treatment) or DMSO. Following treatment, AEA or 2-AG (50 µM) was added to the lysates and the reaction proceeded for 20 min at 37 °C prior to quenching. Hydrolytic activities were determined by quantifying arachidonic acid (AA) production relative to a d_8-arachidonic acid (AA) internal standard by LC-MS/MS. Data represent the mean ± s.e.m. *n* = 3 (K11G9.2 DMSO) or 4 (all other conditions) independent samples per group. **P* = 2.86E-02 (two-sided Mann-Whitney test performed relative to METAP2 or DMSO control). The *P* values are provided in **Supplementary Table 2**.

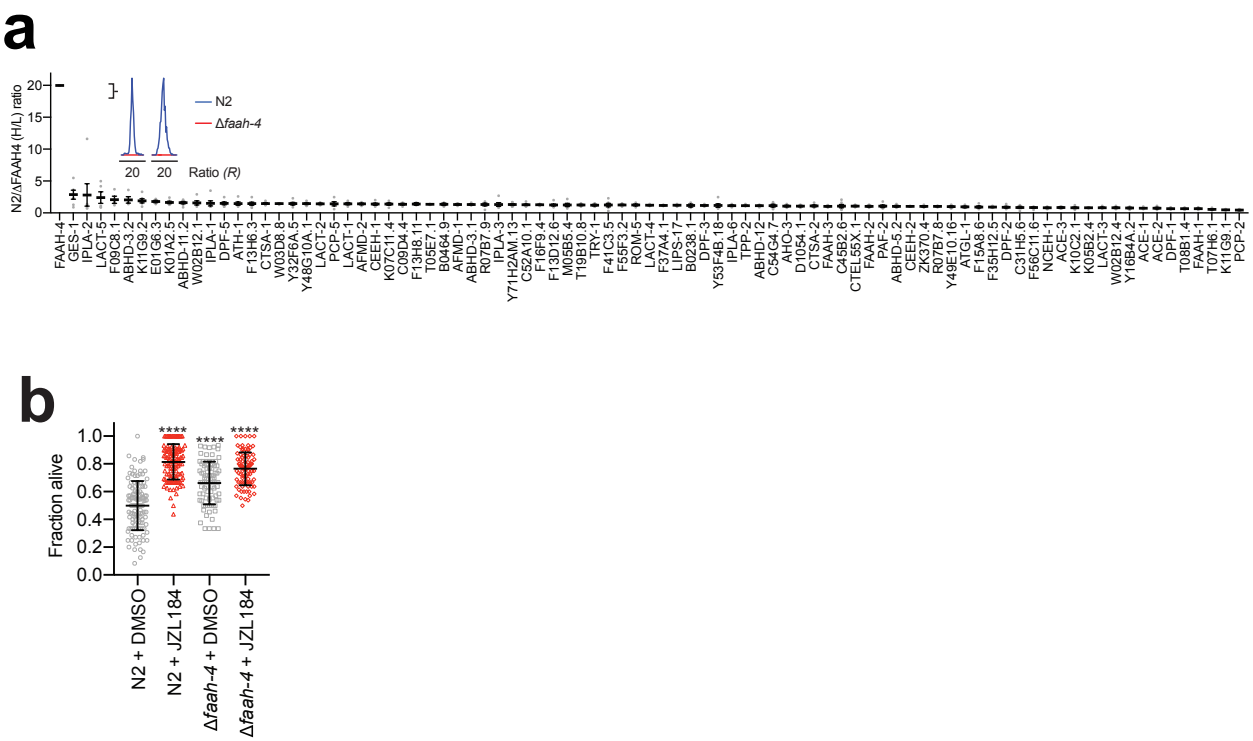

Supplementary Figure 10. Deletion of *faah-4* increases oxidative stress resistance. (**a**) Confirmation of selective loss of FAAH-4 expression in CRISPR/Cas9-based gene knockout of *faah-4* in *C. elegans* by MS-based ABPP. Other SHs were largely unaffected by *faah-4* disruption. Data represent the mean of median ratios + s.e.m. for peptides quantified for each protein (n = 3 independent experiments). (**b**) Loss of FAAH-4 increases resistance to oxidative stress induced by paraquat (50 mM) for 48 hours. Data represent the mean $\pm$ s.d. (N2 DMSO n = 118, N2 JZL184 n = 120, Δ*faah-4* DMSO n = 86, Δ*faah-4* JZL184 n = 93, ****P < 1.00E-15 for N2 JZL184, ****P = 1.24E-10 for Δ*faah-4* DMSO, ****P < 1.00E-15 for Δ*faah-4* JZL184, two-sided Mann-Whitney test performed relative to N2 + DMSO, from 6 independent experiments)

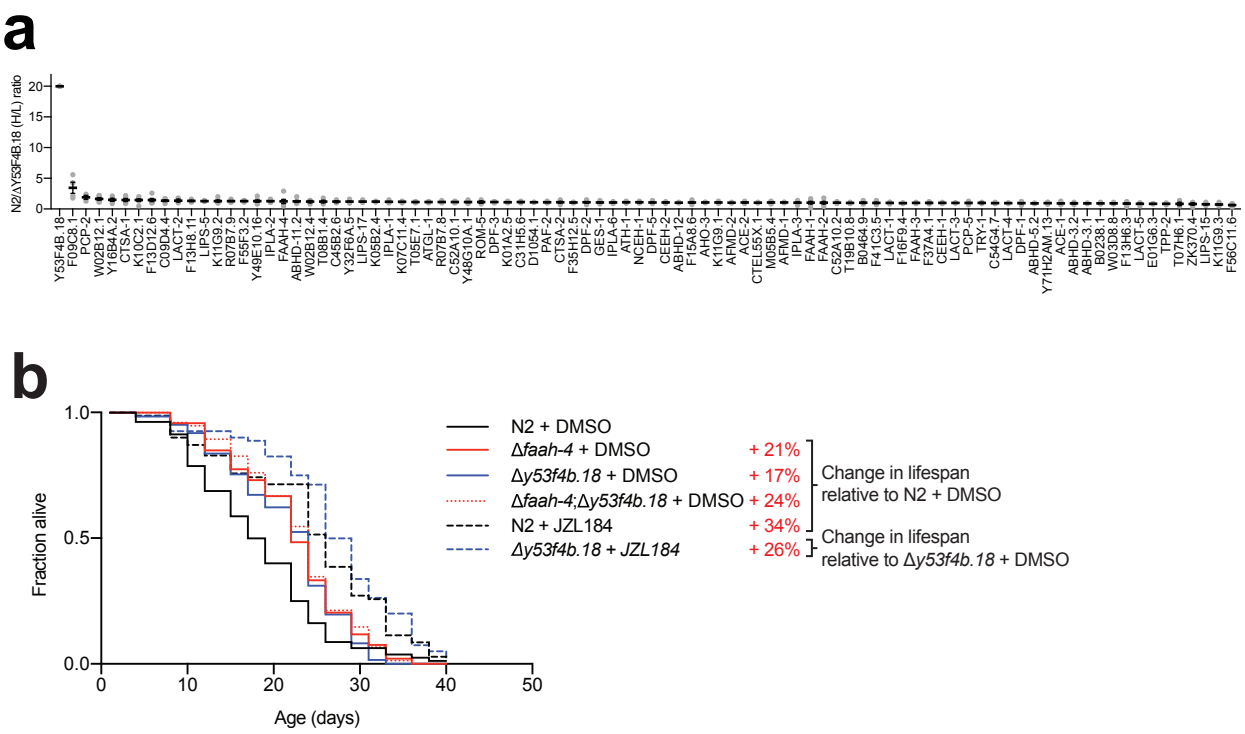

Supplementary Figure 11. Y53F4B.18 regulates lifespan in *C. elegans* and may function within the same pathway as FAAH-4. (**a**) Confirmation of selective loss of Y53F4B.18 in CRISPR/Cas9-based gene knockout of *y53f4b.18* in *C. elegans* by MS-based ABPP. Data represent the mean of median ratios + s.e.m. for peptides quantified for each protein (n = 3 independent experiments). (**b**) Lifespan curves for N2 animals treated with JZL184 (50 μM) or DMSO, Δ*faah-4*, Δ*y53f4b.18* animals treated with JZL184 (50 μM) or DMSO, and Δ*faah-4*;Δ*y53f4b.18. Δfaah-4, Δy53f4b.18, and Δfaah-4*;Δ*y53f4b.18* (N2 DMSO n = 80, Δ*faah*-4 DMSO n = 93, Δ*y53f4b.18* DMSO n = 61, Δ*faah-4*;Δ*y53f4b.18* DMSO n = 75, N2 JZL184 n = 70, Δ *y53f4b.18* JZL184 n = 80, P = 6.38E-03 for N2 DMSO vs Δ*faah*-4 DMSO, P = 3.99E-02 for N2 DMSO vs Δ*y53f4b.18* DMSO, P = 4.12E-03 for N2 DMSO vs Δ*faah-4*;Δ*y53f4b.18* DMSO, P = 6.94E-06 for N2 DMSO vs N2 JZL184, P = 1.99E-07 for Δ*y53f4b.18* DMSO vs Δ*y53f4b.18* JZL184, two-sided Mantel-Haenszel version of the log-rank test). This result is representative of 3 independent experiments. Statistics for **b** are provided in **Supplementary Dataset 2**.

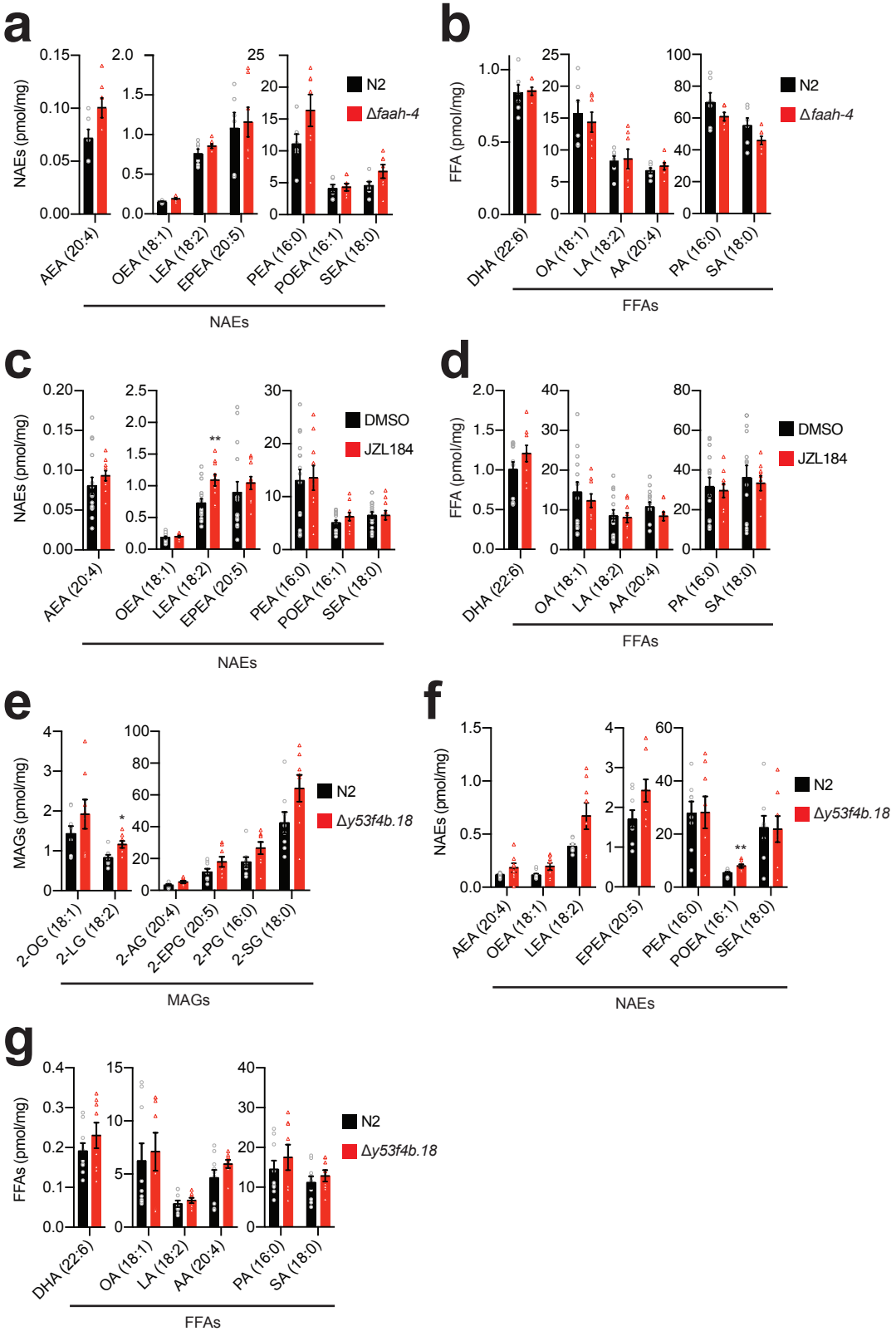

Supplementary Figure 12. Lipids in Δ*faah-4* animals, N2 animals treated with JZL184 and Δ*y53f4b.18* animals. N-acylethanolamines and free fatty acids are largely unchanged in **(a, b)**

Δ*faah-4* animals and animals treated with **(c, d)** JZL184. **(c-e)** MAGs, NAEs and FFAs in Δ*y53f4b.18* animals are mostly unchanged compared to N2 with the exception of POEA and 2-LG. Quantification of lipids from indicated groups of animals was performed by targeted LC-MS/MS. AEA, anandamide (C20:4); OEA, oleoylethanolamide (C18:1); LEA, linoleoyl ethanolamide (C18:2); EPEA, eicosapentaenoyl ethanolamide (C20:5); PEA, palmitoylethanolamide (16:0); POEA, palmitoleoyl ethanolamide (C16:1); SEA, stearoyl ethanolamide (18:0); DHA, docosahexaenoic acid (22:6); OA, oleic acid (18:1); LA, linoleic acid (18:2); PA, palmitic acid (16:0); SA, stearic acid (18:0); AA, arachidonic acid (20:4); 2-OG, 2-oleoylglycerol (C18:1); 2-LG, 2-linoleoylglycerol (C18:2); 2-PG, 2-palmitoylglycerol (C16:0); 2-SG, 2-stearoylglycerol (C18:0); 2-AG, 2-arachidonoylglycerol (C20:4); 2-EPG, 2-eicosapentaenoylglycerol (C20:5). The data represent the mean $\pm$ s.e.m. For **a** and **b**, $n = 6$ (N2) or 7 (Δ*faah-4*) independent samples per group. For **c** and **d**, $n = 9$ (FFAs JZL184), 10 (NAEs JZL184), 14 (FFAs DMSO), or 15 (NAEs DMSO) independent samples per group. For **e** and **g**, $n = 9$ (FFAs N2) or 8 (all other conditions) independent samples per group. $^{**}P < 0.01$ (two-sided Mann-Whitney test performed relative to N2 or DMSO control). The *P* values for **a**-**b**, **c**-**d**, and **e**-**g** are provided in **Supplementary Table 3**, **4** and **5**, respectively.

Supplementary Dataset Legends (see accompanying excel files)

Supplementary Dataset 1. List of predicted *C. elegans* SHs, FP-enriched SHs, and gene expression data, related to Figure 1. (Tab 1): Compiled list of predicted *C. elegans* SHs. UniProtID, WormBase identifier, description, Pfam annotation (family), and sequence are shown for each protein. The list of predicted SHs was generated by cross referencing the proteins with a non-redundant database and identifying *C. elegans* proteins with Pfam families that match curated mammalian SH families. Manually identified entries were added. (Tab 2): List of FP-enriched predicted *C. elegans* SHs with corresponding averaged and median heavy-to-light ratios from 6 independent biological replicates divided into membrane and soluble samples. Combined SILAC ratio, s.d., and s.e.m. were calculated from 12 membrane and soluble replicates. (Tab 3): RNA-Seq data for putative SHs from day 1 *C. elegans* which can be found in the NCBI under the ID code GEO: GSE63528.

Supplementary Dataset 2. Lifespan data. Each tab contains strains, mean lifespan in days, number of animals tested, percent change in lifespan compared to control, and *P*-value. Mean lifespan and *P*-value were calculated by two-sided Mantel-Haenszel version of the log-rank test. Unless stated, compound treatment occurred on day 1 of adulthood. (Tab 1): Inhibitor screen results. Includes percent change in lifespan of animals treated with drug compared to animals treated with DMSO control (corresponding to experiment number). (Tab 2): Top compounds that extend lifespan. Compounds were selected based on initial screen results. Corresponding DMSO data can be found by experiment number. (*n* = 3 biological replicates per compound). (Tab 3): Lifespan statistics from longevity effector mutants treated with JZL184 (50 μM) compared to DMSO (control). ($n \geq 2$ biological replicates per condition) (Tab 4): Lifespan statistics from dose response experiments. Animals were treated with 0.001 to 50 μM JZL184 or DMSO (control). Corresponding DMSO data can be found by experiment number. ($n \geq 3$

biological replicates per concentration of JZL184). (Tab 5): Lifespan statistics from time course experiments. Animals treated with 50 μM JZL184 were compared to animals given DMSO (control) from the L1 developmental stage to day 5 of adulthood. ($n \geq 3$ biological replicates per stage). (Tab 6): Lifespan statistics from JZL184 analogs and CL-01 probe. Corresponding DMSO data can be found by experiment number. ($n \geq 4$ biological replicates per analog). (Tab 7): Lifespan statistics from CL-01 probe. Corresponding DMSO data can be found by experiment number. ($n = 4$ biological replicates). (Tab 8): Lifespan statistics from *faah-4* and *y53f4b.18* deletion animals. Described from top to bottom rows: percent change in lifespan of *faah-4* deletion animals as compared to N2 animals, *y53f4b.18* deletion animals as compared to N2 animals, *faah-4; y53f4b.18* deletion animals as compared to N2 animals, N2 animals treated with JZL184 (50 μM) as compared to DMSO, *faah-4* deletion animals treated with JZL184 (50 μM) as compared to DMSO, *y53f4b.18* deletion animals treated with JZL184 (50 μM) as compared to DMSO, *faah-4; y53f4b.18* deletion animals treated with JZL184 (50 μM) as compared to DMSO, ($n \geq 3$ biological replicates per condition).

Supplementary Dataset 3. Proteomic data, related to Figures 3, 4, and Supplementary Figure 7. (Tab 1-5, 7-8): Competitive ABPP-MS data using FP-biotin (5 μM, 2 h). Average heavy-to-light ratios from experiments in which ^{14}N *C. elegans* were treated with JZL184 (50 μM, 24 h) (Tab 1), ALC1 (50 μM, 24 h) (Tab 2), ALC3 (50 μM, 24 h) (Tab 3), ALC6 (50 μM, 24 h) (Tab 4), WWL154 (50 μM, 24 h) (Tab 5), URB597 (50 μM, 24 h) (Tab 7), or CL-01 (50 μM, 24 h) (Tab 8) and ^{15}N were treated with DMSO (24 h). (Tab 6): Comparative ABPP-MS data using FP-biotin (5 μM, 2 h). Average heavy-to-light ratios from ^{14}N *faah-4* deletion and ^{15}N N2 *C. elegans*. (Tab 9): Competitive ABPP-MS data using CL-01 (50 μM, 18 h). Average heavy-to-light ratios from experiments in which ^{14}N *C. elegans* were treated with JZL184 (50 μM, 24 h) and CL-01 (50 μM, 18 h) and ^{15}N were treated with DMSO (24 h) and CL-01 (50 μM, 18 h). Data are from 2 (ALC1, ALC3), 3 (ALC6, WWL154, Δ*faah-4*, Δ*y53f4b.18*, URB597, JZL184 CL-01, 4

(JZL184), and 6 (CL-01) independent samples. Combined SILAC ratio, s.d., and s.e.m. were calculated from membrane, soluble, and whole lysate replicates.

Supplementary Dataset 4. Proteomic data, related to Figures 3, 4, and Supplementary Table 7. (Tabs 1-34): ABPP-MS data using FP-biotin (5 μM, 2 h) for analysis of *C. elegans* treated with the following compounds at 50 μM for 24 h: JZL184 (Tabs 1-8), ALC1 (Tabs 9-12), ALC 3 (Tabs 13-16), ALC6 (Tabs 17-22), WWL154 (Tabs 23-28), or URB597 (Tabs 29-34). (Tabs 35-40): ABPP-MS data using FP-biotin (5 μM, 2 h) for analysis of *faah-4* deletion animals. (Tabs 41-46): ABPP-MS data using FP-biotin (5 μM, 2 h) for analysis of *y53f4b.18* deletion animals. (Tabs 47-59): ABPP-MS data using CL-01 (50 μM, 24 h) (Tabs 47-53) or JZL184 (50 μM, 24 h) and CL-01 (50 μM, 18 h) (Tabs 54-59). Data sets by replicate, related to **Supplementary Table 3**. Each tab displays the median heavy-to-light ratios for all quantified tryptic peptides per protein.

Supplementary Dataset 5. Proteomic data, related to Figure 3. (Tab 1-2): Averaged heavy-to-light ratios of competitive ABPP-MS data sets for membrane (Tab 1) and soluble (Tab 2) proteomes of *C.elegans* treated with compounds (50 μM, 24 h) using FP-biotin (5 μM, 2 h), related to **Supplementary Table 3**. Includes stdev and number of quantified peptides per condition. Data are from 2 (ALC1, ALC3), 3 (ALC6, WWL154, URB597, JZL184 CL-01, and 4 (JZL184) independent samples.